PHYSICAL REVIEW B **92**, 161115(R) (2015)

Emergence of a Chern-insulating state from a semi-Dirac dispersion

Huaqing Huang,[1,2] Zhirong Liu,[3] Hongbin Zhang,[2] Wenhui Duan,[1,4,5] and David Vanderbilt[2]
[1]*Department of Physics and State Key Laboratory of Low-Dimensional Quantum Physics, Tsinghua University, Beijing 100084, China*
[2]*Department of Physics and Astronomy, Rutgers University, Piscataway, New Jersey 08854-8019, USA*
[3]*College of Chemistry and Molecular Engineering, Peking University, Beijing 100871, China*
[4]*Collaborative Innovation Center of Quantum Matter, Tsinghua University, Beijing 100084, China*
[5]*Institute for Advanced Study, Tsinghua University, Beijing 100084, China*
(Received 3 July 2015; published 28 October 2015)

By combining first-principles calculations with Wannier-based tight-binding modeling, we demonstrate that a TiO_2/VO_2 heterostructure that was previously proposed as a prototypical semi-Dirac system becomes a Chern insulator (quantum anomalous Hall insulator) in the presence of spin-orbit coupling. We show that this occurs only when the semi-Dirac structure is of a special type that can be formed by the merging of three conventional Dirac points. Our results reveal how the nontrivial topology with a nonzero Chern number emerges naturally from this kind of semi-Dirac structure, establishing a general scenario that provides a different route to the formation of Chern-insulating states in practical materials systems.

DOI: 10.1103/PhysRevB.92.161115 PACS number(s): 73.20.−r, 73.21.−b, 73.43.−f

A Chern insulator is a two-dimensional (2D) magnetic insulator with a quantized anomalous Hall conductivity Ce^2/h, where C is an integer topological index known as the Chern number [1]. These systems, also known as quantum anomalous Hall (QAH) insulators, have attracted a great deal of interest, in part because of their gapless chiral edge states which enable dissipationless transport, with potential applications in electronic devices [2]. So far, several systems have been proposed, notably magnetically doped topological insulators [3,4] leading to recent experimental confirmation [5], but also honeycomb [6–11] or square lattices [12–15] formed by transition-metal and heavy-metal ions. The essential ingredients are the spontaneous breaking of time-reversal (TR) symmetry, as by the formation of a ferromagnetic state, and the presence of spin-orbit coupling (SOC), which generates the net Berry curvature needed for a nonzero Chern number. Here we focus on one interesting class of proposals involving 2D systems that would be half semimetals in the absence of SOC, with the Fermi energy pinned at one or more Dirac points in one spin channel while the other channel is gapped. If the application of SOC gaps the Dirac points to produce conical avoided crossings instead, a nonzero Chern number can result, as proposed, for example, for a triphenyl-manganese ($Mn_2C_{18}H_{12}$) system [9].

Recently, calculations on TiO_2/VO_2 multilayer structures led to a proposal [16,17] for a new kind of half semimetal in which, in the absence of SOC, the bands in the ungapped spin channel have a *semi-Dirac* dispersion, i.e., a quadratic rather than a linear dispersion in one direction. This raises the interesting question whether such a system can also provide a route to a Chern-insulating state when SOC is included.

In this Rapid Communication we answer this question. First, we distinguish between two qualitatively different types of semi-Dirac structures. The one we denote as "type I" was proposed in Ref. [18], but we find that it cannot lead to a QAH state. Instead, we find that the TiO_2/VO_2 multilayer structure [16,17] is described by a different "type-II" semi-Dirac cone structure, which does lead to a Chern-insulating state when SOC is turned on. Moreover, we clarify that the type-II structure is not protected by symmetry, and (in the absence of SOC) will generically transform into one or three Dirac nodes in the absence of fine tuning. With SOC, we predict that the TiO_2/VO_2 heterostructure is a QAH insulator with a Chern number of -2, demonstrating a different route to the formation of a Chern-insulating state in 2D.

Dirac and semi-Dirac cones. A general effective two-band Hamiltonian in 2D can be given as

$$H(\mathbf{k}) = \mathbf{h}(\mathbf{k}) \cdot \vec{\sigma}, \tag{1}$$

where $\vec{\sigma} = (\sigma_x, \sigma_y, \sigma_z)$ are Pauli matrices. In 2D $\mathbf{k}$ space a form such as

$$\mathbf{h}(\mathbf{k}) = (v_F k_x, v_F k_y, 0) \tag{2}$$

describes a massless Dirac cone structure, where v_F is the Fermi velocity. Such a form is appropriate in the absence of SOC for a half-semimetal ferromagnet in which the other spin component is gapped out. SOC is taken into account by adding a mass term such that $\mathbf{h}(\mathbf{k}) = (v_F k_x, v_F k_y, m_z)$, opening an energy gap of $2|m_z|$ at the Dirac point. The Chern number is determined by integrating the Berry curvature $\Omega(\mathbf{k})$ over the 2D Brillouin zone (BZ), but for weak SOC the dominant contributions will come from Berry fluxes $\Phi = \pm\pi$ concentrated near the avoided crossings. This follows from the well-known form of the Berry curvature for the two-band model of Eq. (1), which yields

$$\Phi = \int d\mathbf{k}\, \Omega(\mathbf{k}) = \int d\mathbf{k} \frac{\mathbf{h}}{2|\mathbf{h}|^3} \cdot \left(\frac{\partial \mathbf{h}}{\partial k_x} \times \frac{\partial \mathbf{h}}{\partial k_y} \right). \tag{3}$$

Hence each gapped (massive) Dirac cone makes a contribution of $\pm\frac{1}{2}$ to the total Chern number C, which is therefore determined by summing over all the massive Dirac cones at the Fermi level.

On the other hand, a semi-Dirac spectrum is a peculiar energy dispersion in which quasiparticles behave as massless along one principal axis but as massive fermions along the perpendicular direction. Recently, this novel spectrum was observed in a multilayer $(TiO_2)_m/(VO_2)_n$ nanostructure ($m \geqslant 5$; $n = 3$ or 4) by Pardo *et al.* using first-principles calculations [16,17]. They proposed that the semi-Dirac

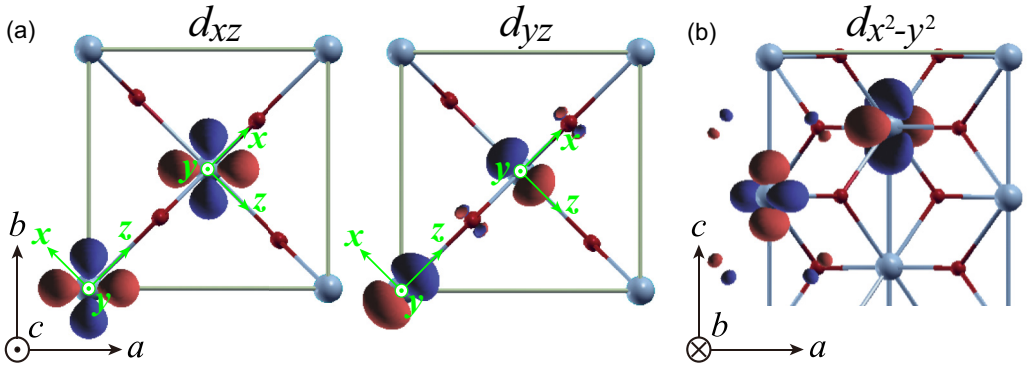

FIG. 1. (Color online) Amplitude isosurfaces of atom-centered d-like maximally localized Wannier functions (red for positive values and blue for negative). (a) $d_\perp$ (yz and xz) and (b) $d_\parallel$ (x^2-y^2) at different V sites in the $(TiO_2)_5/(VO_2)_3$ superlattice. Local coordinate systems are shown in green; local z and y axes are along the in-plane O-V-O chain and the global c axis, respectively.

electronic spectrum could be described by Eq. (1) with [18–20]

$$\mathbf{h}(\mathbf{k}) = \left(\frac{k_x^2}{2m}, v_F k_y, 0\right) \tag{4}$$

or a similar expression. We refer to this model as a "type-I" semi-Dirac model to distinguish it from the "type-II" model we propose below. Obviously the dispersion is massless (linear) along the k_y direction but massive (quadratic) along k_x, satisfying the definition of a semi-Dirac cone. Since Eq. (4) is an even function of k_x, it is evident that the Berry curvature $\Omega(\mathbf{k})$ is an odd function of k_x according to Eq. (3). Hence the Chern number, given by the integral of $\Omega(\mathbf{k})$ over the vicinity of the semi-Dirac point, is zero after adding a mass term $H' = m_z\sigma_z$ to open an energy gap. This is consistent with the observation that the semi-Dirac point under Eq. (4) carries a zero Berry flux [19], in contrast with conventional Dirac points which provide a Berry flux of $\pm\pi$.

We therefore conclude that type-I semi-Dirac cones have a trivial topology with Chern number $C = 0$ and thus do not lead to a Chern-insulating state. Nevertheless, by using first-principles calculations and a Wannier-based tight-binding analysis, we find that SOC does turn the $(TiO_2)_m/(VO_2)_n$ into a Chern insulator. We first present the results and then explain them.

Methods. The first-principles electronic structure calculations are performed within the framework of density functional theory (DFT) [21] as implemented in the QUANTUM ESPRESSO package [22] with the plane-wave pseudopotential method, and in the VASP package [23] with the projector augmented-wave method. We adopted the Perdew-Burke-Ernzerhof generalized gradient approximation (GGA) exchange-correlation functional [24]. The kinetic energy cutoff is fixed to be 500 eV and a Γ-centered $8\times8\times1$ **k**-point mesh is used in all cases. We treat the open-shell $3d$ orbitals by adding an effective Hubbard U correction of 3.4 eV on V and Ti atoms within the GGA+U approach [25,26]. Structural relaxations are carried out without SOC, and then the electronic structure is computed twice, once with and once without SOC. Ferromagnetic ordering is found to be energetically favored in both cases, and the ordering is along the z axis when SOC is present. We use Wannier interpolation based on maximally localized Wannier functions (MLWFs) to calculate the Berry curvature and the anomalous Hall conductivity, which requires a very dense **k**-point grid in the BZ [27,28].

Chern insulator behavior of the $(TiO_2)_5/(VO_2)_3$ system. We focus on the $(TiO_2)_m/(VO_2)_n$ system with $n = 3$ and $m = 5$; because TiO_2 is strongly insulating, the latter is enough to effectively separate the VO_2 trilayers into isolated 2D systems, in which the energy bands close to the Fermi level are dominated by the $3d$ states of V. This multilayer system was fabricated successfully to investigate the metal-insulator transition [29]. Since there are two kinds of VO_6 octahedra whose in-plane O-V-O chains are perpendicular to each other, we align our local axes differently on the two V sites, as shown in Fig. 1(a). Because of the distortion of the VO_6 octahedra away from cubic symmetry, the triply degenerate t_{2g} orbtials of V ions split into two doubly degenerate $d_\perp$ orbtitals (yz and xz) and one $d_\parallel$ orbital (x^2-y^2) [30]. We projected the Bloch wave functions onto these local orbitals to get MLWFs, which serve as an ideal basis for further analyses. As shown in Fig. 1, the MLWFs keep the shape and symmetry of local atomic d orbitals.

Based on these atom-centered d-like MLWFs, we calculate the Wannier-interpolated energy bands close to the Fermi level [31], shown in the top panel of Fig. 2(a). The Wannier-interpolated energy bands are in excellent agreement with the DFT results (not shown). The semi-Dirac character is clearly apparent, with two bands crossing linearly along the Γ-M line and quadratically along A-B (perpendicular to Γ-M). The band crossing in the absence of SOC is protected by the diagonal mirror symmetry of the structure [32]. When SOC is considered in our calculation, an avoided crossing occurs and a small band gap of ~2.5 meV opens at the crossing point. To investigate the topological nature of this system, we calculate the Berry curvature $\Omega(\mathbf{k})$ of all states below the Fermi level using [33]

$$\Omega(\mathbf{k}) = -\sum_{n<E_F}\sum_{m\neq n} 2\,\mathrm{Im}\frac{\langle\psi_{n\mathbf{k}}|v_x|\psi_{m\mathbf{k}}\rangle\langle\psi_{m\mathbf{k}}|v_y|\psi_{n\mathbf{k}}\rangle}{(\varepsilon_{m\mathbf{k}}-\varepsilon_{n\mathbf{k}})^2}, \tag{5}$$

where $\psi_{n\mathbf{k}}$ is the spinor Bloch wave function of band n with corresponding eigenenergy $\varepsilon_{n\mathbf{k}}$, and $\mathbf{v} = (v_x, v_y)$ is the velocity operator. In the bottom panel of Fig. 2(a) the Berry curvature is plotted along the same k path. The large peaks between the Γ and M points arise where the conduction and valence

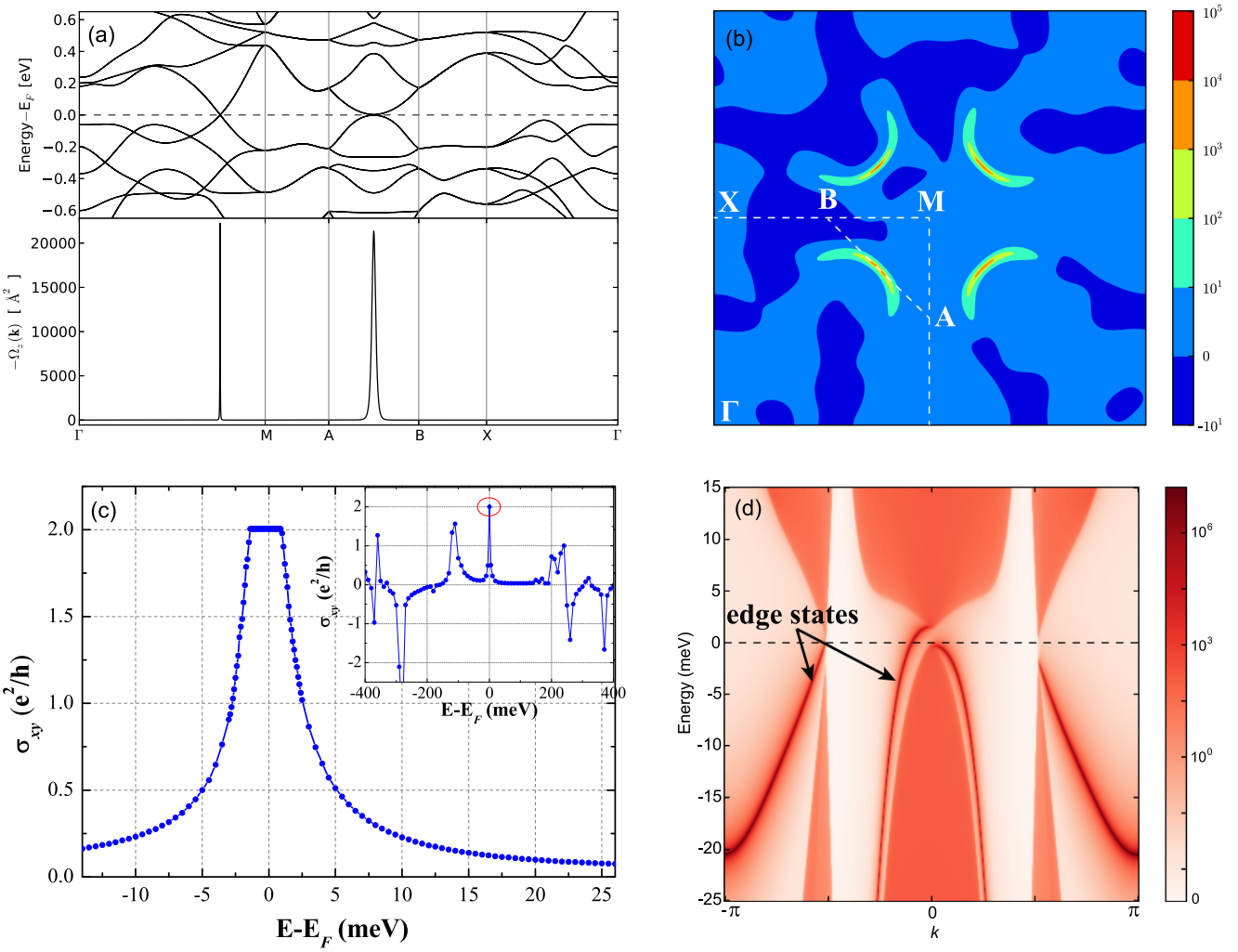

FIG. 2. (Color online) (a) Band structure and Berry curvature $-\Omega(\mathbf{k})$ along and perpendicular to the diagonal of the BZ. (b) Berry curvature $-\Omega(\mathbf{k})$ in the entire BZ. (c) Anomalous Hall conductivity σ_{xy} plotted with respect to the position of the Fermi energy E_F. The inset shows σ_{xy} with E_F varying from -400 to 400 meV. (d) Energy and momentum dependence of the LDOS at the edge along the [11] direction. Note that the color maps are logarithmic; deep blue patches in (b) are numerical artifacts.

bands are nearly degenerate and only weakly split by SOC, giving rise to small denominators in Eq. (5) and hence a large contribution to $\Omega(\mathbf{k})$. The peaks show strong anisotropy, being much sharper along Γ-M than along A-B. The 2D plot in Fig. 2(b) makes it clear that these avoided crossings give rise to four banana-shaped peaks of Berry curvature located around the semi-Dirac points. Note that $\Omega(\mathbf{k})$ is not an odd function along the A-B direction, in contrast with the prediction of Eq. (4). Since the four peaks are related by fourfold rotations, there is no cancellation among them; each contributes a Berry flux of $-\pi$, so that the total Chern number is -2. The system is therefore a Chern insulator. However, it is different from the Chern-insulating phase found in TiO_2/CrO_2 heterostructures [15], which exhibits nearly isotropic Dirac cones instead of semi-Dirac cones.

We also plot the intrinsic anomalous Hall conductivity [34] as a function of Fermi energy in Fig. 2(c). As expected from the nonzero Chern number, the anomalous Hall conductivity shows a quantized Hall plateau at $\sigma_{xy} = -Ce^2/h$ when the Fermi level lies inside the bulk band gap. The width of the Hall plateau is about 2.5 meV, corresponding to the nontrivial bulk band gap. The anomalous Hall conductivity decreases rapidly to zero when the Fermi level is outside the band gap, as expected since only states near the nontrivial bulk band gap, which is opened by the weak SOC, contribute strongly to the Berry curvature [see Figs. 2(a) and 2(b)].

The existence of topologically protected chiral edge states is one of the most important consequences of the QAH state. To further reveal the nontrivial topological nature of the system, we calculate the edge states of a semi-infinite $(TiO_2)_5/(VO_2)_3$ system with its edge along the [11] direction. Because the existence of chiral edge states is completely determined by the bulk topology, here we build the tight-binding model with SOC based on first-principles MLWFs from the bulk, ignoring the effects of edge reconstruction. We apply an iterative method [35] to obtain the edge Green's function and the local density of states (LDOS), which is directly related to the imaginary part of the Green's function. In Fig. 2(d) we can clearly see that two edge states connect the valence and conduction bands. The appearance of two chiral edge states is consistent with our

calculated Chern number $C = -2$, confirming the nontrivial topological nature of this semi-Dirac system.

Type-II semi-Dirac model. The above results demonstrate that the $(TiO_2)_5/(VO_2)_3$ superlattice is undoubtedly a Chern insulator, contrary to previous understandings that a semi-Dirac cone structure should not result in a Chern-insulating state. To resolve such a conflict, we propose a "type-II" semi-Dirac model with an effective 2×2 Hamiltonian in the absence of SOC having the form of Eq. (1) with

$$\mathbf{h}(\mathbf{k}) = \left(\frac{k_x^2}{2m} - v_F k_y, \alpha k_x k_y, 0\right) \tag{6}$$

or other equivalent expressions. As we will show, a type-II Hamiltonian with a similar expression is obtained from our $\mathbf{k}\cdot\mathbf{p}$ analysis of the TiO_2/VO_2 system (for details of the derivation, see the Supplemental Material [32]). The resulting dispersion relation satisfies the semi-Dirac character: It is linear along one direction ($k_x = 0$) and quadratic perpendicular to this direction ($k_y = 0$). Hence the origin point (0,0) is a semi-Dirac point. We then add a SOC-induced mass term $H' = m_z\sigma_z$ to open a gap at the semi-Dirac point.

To understand the nature of the Berry curvature expected from the type-I and type-II models of Eqs. (4) and (6), we plot band dispersions and Berry curvatures derived from these models in Fig. 3. In particular, we investigate the evolution of the crossing points when h_x acquires a small perturbation Δ in both models (assuming $m > 0$ without loss of generality). In the type-I model this leads to the the fusion of two Dirac points as Δ passes through zero. As shown in Figs. 3(a)–3(c), when $\Delta < 0$ there are two Dirac cones located at $\mathbf{k} = (\pm\sqrt{-2m\Delta},0)$; these merge to form a semi-Dirac cone at $\Delta = 0$, and then a gap of magnitude 2Δ appears for $\Delta > 0$. Because the two Dirac points provide Berry fluxes of opposite sign, the total Berry flux vanishes, as shown for $\Delta = 0$ in Fig. 3(g). Thus, the type-I model is topologically trivial, and cannot be used to describe the semi-Dirac structure observed for the $(TiO_2)_5/(VO_2)_3$ superlattice system.

For the type-II model, on the other hand, when $\Delta < 0$ the energy gap vanishes at *three* Dirac points located at $\mathbf{k} = (0,\Delta/v_F)$ and $(\pm\sqrt{-2m\Delta},0)$, as shown in Fig. 3(d). As Δ increases, these approach each other and merge at $\Delta = 0$ into a single semi-Dirac point at $\mathbf{k} = (0,0)$ [Fig. 3(e)]. For $\Delta > 0$, only the touching at $\mathbf{k} = (0,\Delta/v_F)$ remains; the other two points disappear (their coordinates formally become imaginary) [Fig. 3(f)]. Therefore, the type-II semi-Dirac model of Eq. (6) can be viewed as the consequence of the merging of three Dirac points to produce a single Dirac point. Interestingly, more than three Dirac points can also merge together, which happens in bilayer graphene [36]. The distribution of the Berry flux produced by the type-II model at $\Delta = 0$ is shown in Fig. 3(h). Significantly, the Berry curvature near the semi-Dirac point has the banana shape shown in Fig. 3(h), very similar to the DFT results in Fig. 2(b).

For one sign of m_z, the total Berry flux contributed by the type-II model is $+\pi$ independent of Δ; the two Dirac points at $(\pm\sqrt{-2m\Delta},0)$ contribute $+\pi$ when $\Delta < 0$, while the one at $\mathbf{k} = (0,\Delta/v_F)$ switches from $-\pi$ to $+\pi$ as Δ crosses through zero. For the other sign of m_z, all these are reversed. Since there are four symmetry-related semi-Dirac points in the entire BZ, the total Chern number is ± 2. The results of the type-II semi-Dirac model thus agree very well with the DFT calculations of $(TiO_2)_5/(VO_2)_3$ above, strongly suggesting that the type-II model correctly describes this system.

To further verify this conclusion, we conduct an effective $\mathbf{k}\cdot\mathbf{p}$ analysis on the first-principles data without SOC around the band crossing point at (k_c,k_c) and introduce a coordinate

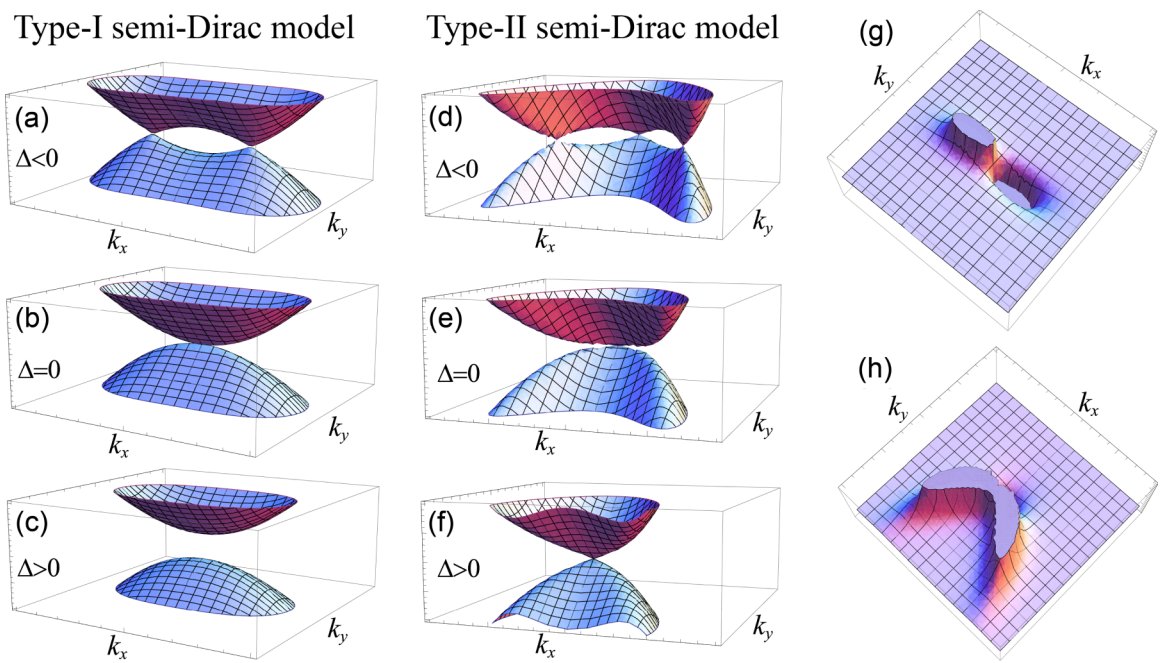

FIG. 3. (Color online) Evolution of band structures of (a)–(c) type-I and (d)–(f) type-II semi-Dirac dispersions when h_x acquires a small perturbation Δ. Berry curvature $-\Omega$ of (g) type-I and (h) type-II semi-Dirac models with $\Delta = 0$ when a SOC-induced mass term $H' = m_z\sigma_z$ is added to open a small gap at the semi-Dirac point.

transformation $\mathbf{q} = (q_1, q_2)$ with $q_1 = (k_x + k_y)/2 - k_c$ and $q_2 = (k_x - k_y)/2$. By employing the downfolding method [37,38], we obtain the 2×2 effective Hamiltonian [32]

$$H_{\mathbf{k}\cdot\mathbf{p}} = \epsilon(\mathbf{q})\mathbb{I}_{2\times 2} + \mathbf{h}(\mathbf{q}) \cdot \vec{\sigma}, \tag{7}$$

where $\mathbb{I}_{2\times 2}$ is the unit matrix. Keeping only terms up to quadratic order in $\mathbf{q}$, we find $\mathbf{h}(\mathbf{q}) = (Aq_1 + Bq_2^2, Cq_2 + Dq_1q_2, 0)$. The coefficient C is small but nonzero, implying that the dispersion along q_2 is almost quadratic, but contains a small linear component. We have checked that the presence of a nonzero coefficient C is not prevented by any symmetry. Setting $\mathbf{h} = \mathbf{0}$ we find three zero-gap Dirac points: a real one at $q_1 = q_2 = 0$ and two virtual ones at $(0.20, \pm 0.56i)$ (in units of a^{-1}, where a is the in-plane lattice constant). These results map onto the Δ-modified type-II model as discussed following Eq. (6), with $q_1 = k_y - \Delta/v_F$ and $q_2 = k_x$, so we can identify $A = -v_F$, $B = 1/2m$, $C = \alpha\Delta/v_F$, and $D = \alpha$. Putting in numbers, we find a small positive Δ, placing the system into the regime of Fig. 3(f), but close to Fig. 3(e). If we artificially decrease C and let it pass through zero, the real and virtual Dirac points merge at $\mathbf{q} = (0,0)$ and reemerge as three real ones, exactly as predicted in Fig. 3(d) for the type-II semi-Dirac model.

We therefore conclude that the $(TiO_2)_5/(VO_2)_3$ nanostructure is an anisotropic linear Dirac system that is so close to a type-II semi-Dirac behavior that it can hardly be distinguished from it. When the system is gapped by SOC, the calculated Berry flux is $\Phi \approx -\pi$ and the Berry curvatures are banana shaped, independent of whether or not the linear term of q_2 is exactly zero [32]. Hence the Chern insulator phase is quite robust, even if the spectrum diverge from the exact semi-Dirac dispersion due to external strain or other perturbations.

Conclusion. We have found that the $(TiO_2)_5/(VO_2)_3$ nanostructure, which exhibits a peculiar semi-Dirac-like electronic structure in the absence of SOC, is a QAH (Chern) insulator with $C = -2$ when SOC is included. The calculated Berry curvature, anomalous Hall conductivity, and gapless edge states unambiguously identify the nontrivial topological nature of this system. We propose a different type-II semi-Dirac model, which describes the semi-Dirac point as the merging of three conventional Dirac points, to explain how a Chern-insulating state is compatible with a semi-Dirac dispersion. Our results clarify when and how the QAH state can emerge from a semi-Dirac structure, providing a potential route to the realization of such states in practical materials systems.

We thank Ivo Souza, Jianpeng Liu, and Wendong Cao for valuable discussions. D.V. is supported by NSF Grant No. DMR-10-05838. H.H., Z.L., and W.D. are supported by the National Natural Science Foundation of China (Grants No. 21373015 and No. 11334006) and the Ministry of Science and Technology of China (Grants No. 2011CB606405 and No. 2011CB921901). H.H. additionally acknowledges the Tsinghua exchange student fund for supporting his visit of Rutgers University.

[1] F. D. M. Haldane, Phys. Rev. Lett. **61**, 2015 (1988).
[2] B. I. Halperin, Phys. Rev. B **25**, 2185 (1982).
[3] C.-X. Liu, X.-L. Qi, X. Dai, Z. Fang, and S.-C. Zhang, Phys. Rev. Lett. **101**, 146802 (2008).
[4] R. Yu, W. Zhang, H.-J. Zhang, S.-C. Zhang, X. Dai, and Z. Fang, Science **329**, 61 (2010).
[5] C.-Z. Chang, J. Zhang, X. Feng, J. Shen, Z. Zhang, M. Guo, K. Li, Y. Ou, P. Wei, L.-L. Wang, Z.-Q. Ji, Y. Feng, S. Ji, X. Chen, J. Jia, X. Dai, Z. Fang, S.-C. Zhang, K. He, Y. Wang, L. Lu, X.-C. Ma, and Q.-K. Xue, Science **340**, 167 (2013).
[6] Z. Qiao, S. A. Yang, W. Feng, W.-K. Tse, J. Ding, Y. Yao, J. Wang, and Q. Niu, Phys. Rev. B **82**, 161414 (2010).
[7] D. Xiao, W. Zhu, Y. Ran, N. Nagaosa, and S. Okamoto, Nat. Commun. **2**, 596 (2011).
[8] H. Zhang, C. Lazo, S. Blügel, S. Heinze, and Y. Mokrousov, Phys. Rev. Lett. **108**, 056802 (2012).
[9] Z. F. Wang, Z. Liu, and F. Liu, Phys. Rev. Lett. **110**, 196801 (2013); H. Hu, Z. Wang, and F. Liu, Nanoscale Res. Lett. **9**, 690 (2014).
[10] K. F. Garrity and D. Vanderbilt, Phys. Rev. Lett. **110**, 116802 (2013).
[11] G.-F. Zhang, Y. Li, and C. Wu, Phys. Rev. B **90**, 075114 (2014).
[12] H. Zhang, J. Wang, G. Xu, Y. Xu, and S.-C. Zhang, Phys. Rev. Lett. **112**, 096804 (2014).
[13] K. F. Garrity and D. Vanderbilt, Phys. Rev. B **90**, 121103 (2014).
[14] H. Zhang, H. Huang, K. Haule, and D. Vanderbilt, Phys. Rev. B **90**, 165143 (2014).
[15] T. Cai, X. Li, F. Wang, S. Ju, J. Feng, and C.-D. Gong, Nano Lett. **15**, 6434 (2015).
[16] V. Pardo and W. E. Pickett, Phys. Rev. Lett. **102**, 166803 (2009).
[17] V. Pardo and W. E. Pickett, Phys. Rev. B **81**, 035111 (2010).
[18] S. Banerjee, R. R. P. Singh, V. Pardo, and W. E. Pickett, Phys. Rev. Lett. **103**, 016402 (2009).
[19] G. Montambaux, F. Piéchon, J.-N. Fuchs, and M. O. Goerbig, Phys. Rev. B **80**, 153412 (2009); Eur. Phys. J. B **72**, 509 (2009).
[20] S. Banerjee and W. E. Pickett, Phys. Rev. B **86**, 075124 (2012).
[21] P. Hohenberg and W. Kohn, Phys. Rev. **136**, B864 (1964).
[22] P. Giannozzi *et al.*, J. Phys.: Condens. Matter **21**, 395502 (2009); http://www.quantum-espresso.org.
[23] G. Kresse and J. Furthmüller, Comput. Mater. Sci. **6**, 15 (1996); http://www.vasp.at.
[24] J. P. Perdew, K. Burke, and M. Ernzerhof, Phys. Rev. Lett. **77**, 3865 (1996).
[25] V. I. Anisimov, J. Zaanen, and O. K. Andersen, Phys. Rev. B **44**, 943 (1991).
[26] S. L. Dudarev, G. A. Botton, S. Y. Savrasov, C. J. Humphreys, and A. P. Sutton, Phys. Rev. B **57**, 1505 (1998).
[27] N. Marzari and D. Vanderbilt, Phys. Rev. B **56**, 12847 (1997); I. Souza, N. Marzari, and D. Vanderbilt, *ibid.* **65**, 035109 (2001).
[28] A. A. Mostofi, J. R. Yates, Y.-S. Lee, I. Souza, D. Vanderbilt, and N. Marzari, Comput. Phys. Commun. **178**, 685 (2008).
[29] K. Shibuya, M. Kawasaki, and Y. Tokura, Phys. Rev. B **82**, 205118 (2010).

[30] J. B. Goodenough, J. Solid State Chem. **3**, 490 (1971).
[31] J. R. Yates, X. Wang, D. Vanderbilt, and I. Souza, Phys. Rev. B **75**, 195121 (2007).
[32] See Supplemental Material at http://link.aps.org/supplemental/10.1103/PhysRevB.92.161115 for more computation details, the derivation of the $\mathbf{k}\cdot\mathbf{p}$ model, and a detailed analysis of the electronic structure.
[33] X. Wang, J. R. Yates, I. Souza, and D. Vanderbilt, Phys. Rev. B **74**, 195118 (2006).
[34] N. Nagaosa, J. Sinova, S. Onoda, A. H. MacDonald, and N. P. Ong, Rev. Mod. Phys. **82**, 1539 (2010).
[35] M. P. López Sancho, J. M. López Sancho, and J. Rubio, J. Phys. F **14**, 1205 (1984); **15**, 851 (1985).
[36] R. de Gail, J.-N. Fuchs, M. O. Goerbig, F. Piéchon, and G. Montambaux, Physica B **407**, 1948 (2012).
[37] I. V. Solovyev, Z. V. Pchelkina, and V. I. Anisimov, Phys. Rev. B **75**, 045110 (2007).
[38] H. Huang, W. Duan, and Z. Liu, New J. Phys. **15**, 023004 (2013).